Mid-infrared sensor based on suspended microracetrack resonator with lateral sub-wavelength-grating metamaterial cladding

Zecen Zhang,[1] Geok Ing Ng,[1] Ting Hu,[1] Haodong Qiu,[1] Xin Guo,[1] Wanjun Wang,[1] Mohamed S. Rouifed,[1] Chongyang Liu,[1] Jiaxu Sia,[1] Jin Zhou,[1] Callum G. Littlejohns,[1,2] Graham T. Reed[2] and Hong Wang[1]

[1]Silicon Technologies, Centre of Excellence, School of Electrical and Electronic Engineering, Nanyang Technological University, 639798 Singapore
[2]Optoelectronics Research Centre, University of Southampton, Southampton, SO17 1BJ, UK.

DOI: XXXX/JPHOT.2017.XXXXXXX
1943-0655/$25.00 ©2017 IEEE

Manuscript received XXX; revised XXX; accepted XXX. Date of publication XXX; date of current version XXX. This work was supported in part by the National Research Foundation Singapore under Grant NRF-CRP12-2013-04 and in part by the Nanyang Technological University-A*Star Silicon Technologies Centre of Excellence. Corresponding author: Geok Ing Ng (e-mail: EGING@ntu.edu.sg).

Abstract: A mid-infrared (MIR) bio-chemical sensor based on a one-time Si etching suspended microracetrack resonator with lateral sub-wavelength-grating (SWG) metamaterial cladding is theoretically and experimentally demonstrated on a commercial 340 nm-thick-top-silicon silicon-on-insulator (SOI) platform. The suspended structure offers an increased interaction area between the mode field and the chemicals under investigation, as well as good sensitivity. The one-time Si etching process also eases the fabrication. The suspended waveguide is optimized to obtain a balance between propagation loss and sensitivity. The suspended microracetrack resonator is experimentally measured at 2 μm wavelength with an extinction ratio (ER) of 12.1 dB and a full-width-at-half-maximum (FWHM) of 0.13 nm, which corresponds to a quality factor (Q factor) of 15300. With the equivalent refractive index method and a specially developed numerical model, the sensing performance based on the waveguide structure has been simulated and analyzed. The simulation results show that the expected sensitivity of fundamental TE mode can achieve 337.5 nm/RIU. This one-time Si etching suspended microracetrack resonator shows great potential for ultra-sensitive MIR optical bio-chemical sensing applications.

Index Terms: Silicon nanophotonics, Waveguide devices, Sensors.

1. Introduction

In the last several decades, silicon photonics based on the silicon-on-insulator (SOI) platform has attracted a lot of research interest, because it can utilize the mature fabrication processes developed within the CMOS industry, resulting in low cost fabrication. A great deal of effort has been invested in SOI based bio-chemical sensing in the near-infrared (NIR) band, typically around 1.3-1.6 μm wavelength [1-6]. Various structures have been utilized to achieve high sensitivity. In 2014, Sahba Talebi Fard et al. obtained a sensitivity of 100 nm/RIU with a TE resonator sensor based on ultra-thin Si waveguides [7]. Series' of slot-waveguide-based microring sensors have been reported to reach a sensitivity of 298 nm/RIU [8-10]. Additionally, sub-wavelength-grating waveguide-based microring sensors have been demonstrated to achieve a sensitivity as high as 490 nm/RIU [11-15]. The mid-infrared (MIR) band (2–20 μm) is also very

crucial in analyzing and sensing various important organic and inorganic materials as their molecules have vibration modes with frequency fingerprints in this band [16-18]. However, limited work has been reported on SOI platform based MIR sensors. One of the limitations of MIR sensing based on the SOI platform is the large optical absorption in buried-oxide-layer (BOX) at wavelengths beyond 4 μm. One solution to this problem is to form suspended structures with the BOX layer etched away, which can also enhance the interaction between the mode field and the material under test, and therefore increase the sensitivity of the device [19-22]. In 2012, Z. Cheng et al. claimed a suspended membrane waveguide based microring resonator operating at 2.75 μm [23]. In 2013, Y. Xia et al. experimentally reported a suspended Si resonator operating at 3.4 μm and 5.2 μm [24]. However, to form their structures, multiple etching processes are required, including a partial Si etching to form the rib waveguides and a Si full etching to form the via-holes for the subsequent hydrofluoric acid (HF) etching of the BOX layer. Furthermore, the wide and thin slabs supporting the rib waveguides, which aim to suppress the mode leakage, provide limited mechanical stability.

In this manuscript, we theoretically and experimentally demonstrate a MIR bio-chemical sensor based on a one-time Si etching suspended microracetrack resonator with a lateral sub-wav elength-grating (SWG) metamaterial cladding on a commercial SOI platform. A quality factor (Q factor) of 15300 and an extinction ratio (ER) of 12.1 dB were obtained at 2 μm wavelength. Furthermore, we have also calculated and analyzed the influence of three important parameters (the duty-cycle of the SWG cladding, the thickness of the waveguides and the width of the waveguides) on the sensitivity with a specially developed numerical model. The expected sensitivity of the fundamental TE mode is calculated to be 337.5 nm/RIU. Compared with the state-of–the-art reported data, this system shows great potential for sensing applications in the MIR band.

2. Device Designs, Fabrication and Characterization

The one-time Si etching suspended microracetrack resonators with lateral SWG metamaterial claddings are designed on a commercial SOI wafer with 340 nm-thick-top-silicon and 2 μm-thick BOX layer. The cladding layer is air. At first, designing and optimizing the fundamental building block, namely the suspended waveguide, as shown in Fig. 1, was carried out.

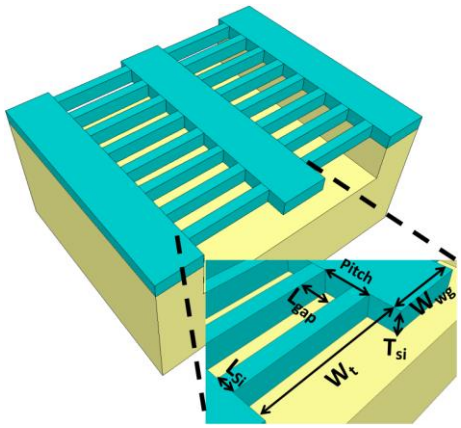

Fig. 1. The schematic of the one-time Si etching suspended waveguide with lateral SWG metamaterial cladding.

For the optimization of the suspended waveguide, three crucial points need to be addressed: (1) diffractive effect and back-reflections caused by the SWG structure; (2) mechanical stability; and (3) enhancement of the interaction between the evanescent field and the chemicals under test. Firstly, in order to suppress the diffractive effect and back-reflections caused by the SWG structure, the pitch of the SWG ($Pitch = L_{si} + L_{gap}$) needs to follow the Bragg condition [21]:

This article has been accepted for publication in a future issue of this journal, but has not been fully edited. Content may change prior to final publication. Citation information: DOI 10.1109/JPHOT.2018.2809662, IEEE Photonics Journal

$$Pitch < Pitch_{Bg} = \frac{\lambda}{2n_{B-F}} \quad (1)$$

where $Pitch_{Bg}$ is the Bragg period; λ is the operating wavelength; and n_{B-F} is the effective index of the fundamental Bloch-Floquet mode propagating in the waveguide. Secondly, in order to obtain a mechanically robust structure to overcome the fluctuations caused by testing liquid or gas flow, wide silicon pillars are required. However, it is known that the sensitivity is determined by the interaction between the evanescent field and the chemicals under test [25]. The trade-off is that whilst the pitch is fixed and the duty-cycle ($DC = L_{si} / (L_{si} + L_{gap}) = L_{si} / Pitch$) increases, the exposed area of waveguide becomes smaller, as well as the overlap between the evanescent field and the chemicals under test, which results in the degradation of sensitivity. So a balance between mechanical stability and sensitivity needs to be considered under the precondition of a small enough $Pitch$ that can suppress the diffractive effect and back-reflections caused by the SWG structure. The width of the lattice is set as 2 μm to prevent lateral mode leakage. Two further important parameters are the width and the thickness of the waveguides. A shrink of the waveguide cross-section area will compress the mode field. Consequently, more energy will gather at the surface of the waveguide, thus bringing a stronger interaction between the evanescent field and the chemicals under test, but at the expense of a higher propagation loss. This is another trade-off to be considered when designing the device.

In order to test and verify the above discussions, suspended waveguides with different dimensions were fabricated on a commercial SOI wafer with a 340 nm-thick-top-silicon layer and a 2 μm BOX layer. The waveguide and SWG cladding are simultaneously defined with electron beam lithography (EBL), and subsequently fully etched to the BOX layer with deep reactive ion etching (DRIE) in order to have a straight and smooth sidewall. Finally, the BOX layer is removed with buffered oxide etching (BOE) solution (6 parts 40% NH_4F and 1 part 49% HF) for 25 minutes at an average etch rate of ~ 65 nm/min.

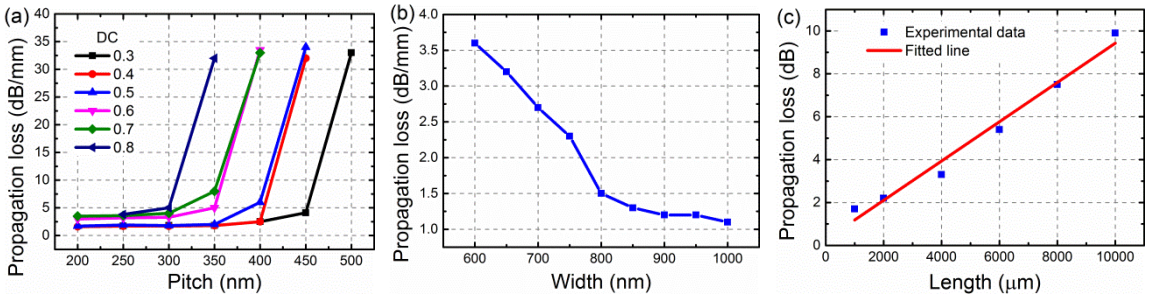

Fig. 2. (a) The propagation loss under different DC and Pitch when W_{wg} = 800 nm and T_{si} = 340 nm. (b) The propagation loss under different W_{wg} when DC = 0.3, Pitch = 350 nm and T_{si} = 340 nm. (c) The experimental measured propagation loss and fitted line when DC = 0.3, Pitch = 350 nm, W_{wg} = 800 nm and T_{si} = 340 nm.

All the characterizations in this manuscript were conducted under room temperature. The input light was generated with a Thorlabs FP laser diode and then coupled into a single-mode optical fiber. The polarization of the input light was tuned to be fundamental TE mode with an in-line polarization controller. With two symmetric fiber holders on the input and output 5-axis stages, the input and output angle of the fibers were tuned as 13° from vertical in order to fit the design of our grating couplers. At the output side, an Artifex extended InGaAs photodetector was utilized to measure the output power. Subsequently, the transmission spectra were plotted.

As shown in Fig. 2(a), when DC = 0.3, $Pitch$ > 450 nm, the propagation loss suddenly increases significantly and reaches the limitation of our detector (-32 dB) due to the serious diffractive effect and back reflections caused by the SWG supporting structure. With an increase of DC to 0.8, the cut-off point moves to smaller pitches, which is consistent with the reported simulation results [21]. In order to avoid the diffractive effect and back reflections whilst retaining a large exposed waveguide area, we choose the dimensions as $Pitch$ = 350 nm and DC = 0.3. Fig. 2(b) shows the influence of the waveguide width on the propagation loss with $Pitch$ = 350

nm and DC = 0.3. As seen, with the increase of width from 600 nm to 800 nm, the propagation loss drops dramatically. But with further width increases, the propagation loss does not decrease significantly. Although wider waveguides (W_{wg} > 800 nm) can offer better mode confinement and slightly lower propagation losses, the sensor sensitivity is degraded by a reduction in the interaction between the evanescent field and the chemicals under test. As a result, we set W_{wg} = 800 nm in order to have a balance between the propagation loss and the sensitivity. Due to the limitation of experimental setup, the impact of the thickness is investigated by simulations instead of experiments, which will be demonstrated in section 3. With all the above optimized parameters and T_{si} = 340 nm, the propagation loss has been plotted and fitted in Fig. 2(c). As seen, the propagation loss of the one-time Si etching suspended waveguide is approximately 9.2 dB/cm.

Based on the above suspended waveguides ($Pitch$ = 350 nm, DC = 0.3, W_{wg} = 800 nm, and T_{si} = 340 nm), the suspended microracetrack resonator was fabricated and characterized. The scanning electron microscope (SEM) images of the fabricated device are shown in Fig. 3. The coupling length (CL) and the gap width (W_g) between the bus waveguide and the microracetrack are 10 μm and 200 nm respectively. The bend radius (R) is 50 μm. The shadow area at the outside of the lattice is due to the removal of the BOX layer with a width of ~1.6 μm. Since the etching of BOE is isotropic, it can be confirmed that the waveguide is fully suspended.

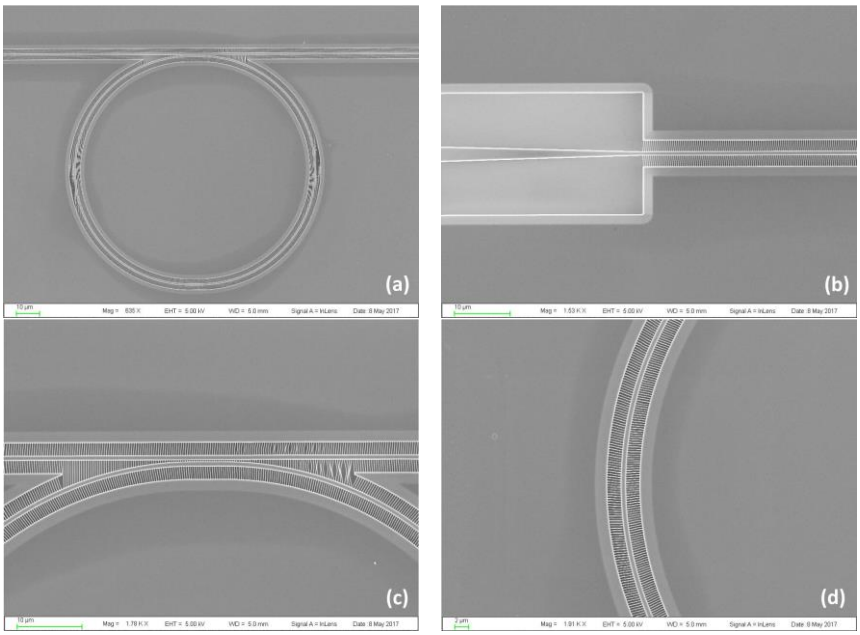

Fig. 3. SEM images of (a) The one-time Si etching suspended microracetrack resonator. (b) The transition region. (c) The coupling region. (d) The microracetrack bend.

The experimental and theoretical fitting results are shown in Fig. 4. The fitting numerical model is specially developed with the equivalent refractive index model. The equivalent refractive index model is a convenient and helpful approach for facilitating the design of SWG based structures, which has been utilized and validated in many reported works [14,15,26-33]. But it needs to be noted that this approach is a narrowband approximation, especially when the dimensions of the SWG are close to the Bragg condition as shown in equation (1). For an accurate broadband simulation, full 3D-FDTD simulations or some more complex numerical models as reported in [34-41] should be used. Here, since $Pitch$ = 350 nm is far smaller than the Bragg period and the calculation is conducted in a narrowband (1995-2005 nm), the equivalent refractive index model can be applied for the lateral SWG cladding metamaterial, which can be written as:

$$n_{eq} = n_{cladding} + DC*(n_{si} - n_{cladding}) \quad (2)$$

where $n_{cladding}$ is the refractive index of the cladding layer, such as the chemicals under test; and

n_{si} is the refractive index of silicon. With this equivalent refractive index of the lateral cladding layer, the effective indices of the suspended waveguide at different wavelengths can be calculated with the BeamPROP module of Rsoft software by taking the dispersion into account. Then, by substituting the effective indices into our numerical model and tuning the coupling coefficient k and round-trip power attenuation α^2, the fitted transmission spectrum can be obtained. The fitting parameters are: k = 0.41i and α^2 = 0.895. From the measurements, the full-width-at-half-maximum (FWHM) is approximately 0.13 nm, which corresponds to a Q factor of ~15300. The ER is approximately 12.1 dB.

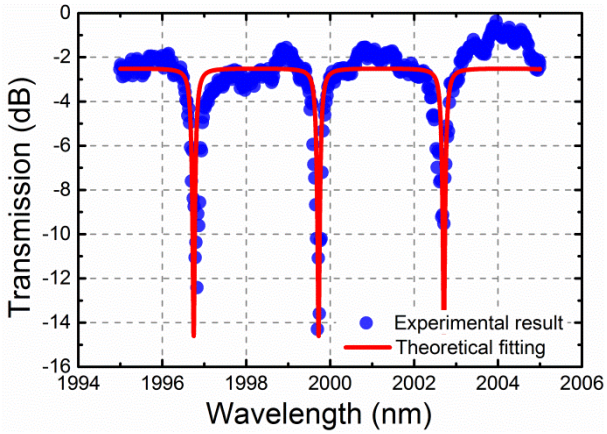

Fig. 4. The experimental and theoretical fitting results of the one-time Si etching suspended microracetrack resonator with SWG metamaterial cladding with CL = 10 μm, W_g = 200 nm, and R = 50 μm.

3. Device Performance Discussion

With the equivalent refractive index method and our numerical model, the expected sensitivity for the microracetrack resonator can be calculated. Here, we calculate the sensitivity of our device to ethanol-water solutions of different concentrations (0% ~ 4%). The refractive index of pure water is 1.306 at 2 μm wavelength. When the concentration increases by 1%, the refractive index of the ethanol-water solution increases by 0.00047. As demonstrated in equation (2), DC will directly influence the equivalent refractive index of the lateral cladding metamaterial, and consequently impact the device sensitivity. Additionally, W_{wg} and T_{si} also influence the sensitivity by compressing the mode field and changing the interaction between the evanescent field and the chemicals under test. So here we mainly discuss the impact of these three factors on the sensitivity. In all the simulations, the other parameters are fixed as: k = 0.35i and α^2 = 0.9331. Through calculating the transmission spectra with the ethanol-water solution cladding of different concentrations and measuring the wavelength shifts of the microracetrack resonant dip, the sensitivities can be obtained. As shown in Fig. 5(a), when DC increases, the sensitivity of the fundamental TE mode decreases as the exposed area to the chemicals under test becomes smaller. Furthermore, it can be seen that the sensitivity when W_{wg} = 600 nm is higher than when W_{wg} = 800 nm. This is because, when W_{wg} is smaller, the fundamental TE mode is more compressed and the field energy is closer to the side walls, which results in a stronger interaction between the evanescent field and the chemicals under test. However, more energy gathering at the side walls also leads to a larger impact from the dimensions of the corrugations, such as DC, which is the reason why the total decrease of sensitivity when W_{wg} = 600 nm is also larger than W_{wg} = 800 nm. As demonstrated in Fig. 5(b), with the increase of W_{wg} from 600 nm to 1000 nm, the sensitivity of the fundamental TE mode drops by ~46.7%. This is due to the fact that when the width increases, the confinement of the mode field is stronger, and the interaction between the evanescent field and the chemicals under test becomes weaker. As seen in Fig. 5(c), with an increase in thickness, the sensitivity of the fundamental TE mode drops considerably. Meanwhile, the decreasing rate of the sensitivity gradually reduces. This is because when the thickness is

small and the mode field is compressed, the interaction between the evanescent field and the chemicals occurring at the upper and the lower surfaces of the waveguide is much stronger compared to when the thickness is larger. It is noteworthy that when T_{si} = 120 nm, the expected sensitivity of the fundamental TE mode can achieve 337.5 nm/RIU. This sensitivity is more than 3 times the reported ultra-thin TE resonator sensor (100nm/RIU) [7], and is comparable to the reported slot-waveguide-based microring sensors (298 nm/RIU) [8-10]. Although the sensitivity is lower than the reported SWG waveguide-based microring sensors (490 nm/RIU) [11-15], the advantage of this suspended microracetrack resonator sensor is that it can avoid absorption from the BOX layer, especially when one extends the use of this structure to longer wavelengths in the MIR band.

Furthermore, as the change of thickness has a larger impact on the mode field in the vertical direction than the lateral direction, the sensitivity of the fundamental TM mode has a larger benefit than the fundamental TE mode from the same reduction of the waveguide thickness. Hence, a higher sensitivity of the fundamental TM mode can be expected. Besides, by utilizing post-fabrication treatments, such as piranha etch/HF cycling and annealing, the surface roughness and therefore the round-trip propagation loss can be reduced, leading to a further improved sensitivity.

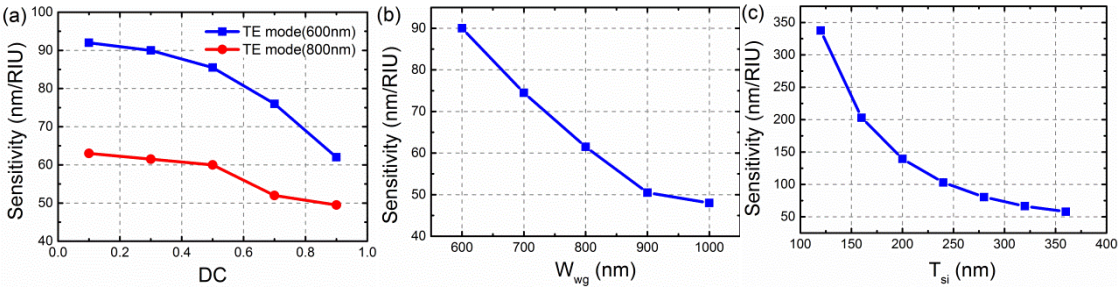

Fig. 5. (a) The sensitivities of fundamental TE mode under different DC when W_{wg} is 600 nm and 800 nm (T_{si} = 340 nm). (b) The sensitivities of fundamental TE mode at different W_{wg} when DC = 0.3 and T_{si} = 340 nm. (c) The sensitivities of fundamental TE mode under different T_{si} when DC = 0.3 and W_{wg} = 800 nm.

4. Conclusion

For the first time, we have theoretically and experimentally demonstrated a MIR sensor based on a one-time Si etching suspended microracetrack resonator with lateral SWG metamaterial cladding. With the suspended structure, the interaction between the evanescent field and the chemicals under test is enhanced, which is helpful for improving the sensitivity. The one-time Si etching process also simplifies the device fabrication. Various suspended waveguides with different dimensions were fabricated and characterized. The propagation loss of the optimized suspended waveguide is experimentally measured as ~9.2 dB/cm. Based on the optimized suspended waveguide, the one-time Si etching suspended microracetrack resonator was fabricated and tested. The experimental data is well fitted with our specially developed numerical model. The ER of the suspended microracetrack resonator is ~12.1 dB. The FWHM is approximately 0.13 nm, which corresponds to a Q factor of ~15300. With the equivalent refractive index method and our numerical model, the influence of three key parameters on the sensitivity are simulated and analyzed. The expected sensitivity of the fundamental TE mode is calculated as 337.5 nm/RIU. The results presented in this paper show great potential for ultra-sensitive, simple to fabricate, low cost MIR integrated optical bio-chemical sensing applications.

References

[1] K. D. Vos, I. Bartolozzi, E. Schacht, P. Bienstman, and R. Baets, "Silicon-on-Insulator microring resonator for sensitive and label-free biosensing," *Opt. Express,* vol. 15, no. 12, pp. 7610-7615, 2007.

[2] K. D. Vos, J. Girones, S. Popelka, E. Schacht, R. Baets, and P. Bienstman, "SOI optical microring resonator with poly(ethylene glycol) polymer brush for label-free biosensor applications," *Biosensors and Bioelectronics*, vol. 24, no. 8, pp. 2528–2533, 2009.

[3] A. L. Washburn, L. C. Gunn, and R. C. Bailey, “Label-free quantitation of a cancer biomarker in complex media using silicon photonic microring resonators,” *Anal. Chem.*, vol. 81, no. 22, pp. 9499–9506, 2009.
[4] A. L. Washburn, M. S. Luchansky, A. L. Bowman, and R. C. Bailey, “Quantitative, label-free detection of five protein biomarkers using multiplexed arrays of silicon photonic microring resonators,” *Anal. Chem.,* vol. 82, no. 1, pp. 69–72, 2010.
[5] J. G. W.-Pérez, P. Cheben, A. Ortega-Moñux, C. A.-Ramos, D. P.-Galacho, R. Halir, I. M.-Fernández, D.-X. Xu, and J. H. Schmid, "Evanescent field waveguide sensing with subwavelength grating structures in silicon-on-insulator," *Opt. Lett.*, vol. 39, no. 15, pp. 4442-4445, 2014.
[6] X. Wang, J. Flueckiger, S. Schmidt, S. Grist, S. T. Fard, J. Kirk, M. Doerfler, K. C. Cheung, D. M. Ratner, and L. Chrostowski, “A silicon photonic biosensor using phaseshifted Bragg gratings in slot waveguide,” *J. Biophoton.*, vol. 6, no. 10, pp. 821-828, 2013.
[7] S. T. Fard, V. Donzella, S. A. Schmidt, J. Flueckiger, S. M. Grist, P. T. Fard, Y. Wu, R. J. Bojko, E. Kwok, N. A. F. Jaeger, D. M. Ratner, and L. Chrostowski, "Performance of ultra-thin SOI-based resonators for sensing applications," *Opt. Express*, vol. 22, no. 12, pp. 14166-14179, 2014.
[8] W. C. Jiang and Q. Lin, "Suspended silicon slotted microring resonators with ultra-high optical quality," *Proc. SPIE*, vol. 9367, Silicon Photonics X; pp. 936708, 2015.
[9] T. Claes, J. G. Molera, K. D. Vos, E. Schacht, R. Baets. and P. Bienstman, “Label-free biosensing with a slot waveguide-based ring resonator in silicon on insulator,” *IEEE Photonics J.*, vol. 1, no. 3, pp. 197–204, 2009.
[10] K. B. Gylfason, C. F. Carlborg, A. Kaźmierczak, F. Dortu, H. Sohlström, L. Vivien, C. A. Barrios, W. V. D. Wijngaart, and G. Stemme, "On-chip temperature compensation in an integrated slot-waveguide ring resonator refractive index sensor array," *Opt. Express*, vol. 18, no. 4, pp. 3226-3237, 2010.
[11] P. J. Bock, P. Cheben, J. H. Schmid, J. Lapointe, A. Delâge, S. Janz, G. C. Aers, D.-X. Xu, A. Densmore, and T. J. Hall, "Subwavelength grating periodic structures in silicon-on-insulator: a new type of microphotonic waveguide," *Opt. Express*, vol. 18, no. 19, pp. 20251-20262, 2010.
[12] J. Wang, I. Glesk, and L. R. Chen, "Subwavelength grating filtering devices," *Opt. Express*, vol. 22, no. 13, pp. 15335-15345, 2014.
[13] V. Donzella, A. Sherwali, J. Flueckiger, S. T. Fard, S. M. Grist, and L. Chrostowski, "Sub-wavelength grating components for integrated optics applications on SOI chips," *Opt. Express*, vol. 22, no. 17, pp. 21037-21050, 2014.
[14] V. Donzella, A. Sherwali, J. Flueckiger, S. M. Grist, S. T. Fard, and L. Chrostowski, "Design and fabrication of SOI micro-ring resonators based on sub-wavelength grating waveguides," *Opt. Express*, vol. 23, no. 4, pp. 4791-4803, 2015.
[15] J. Flueckiger, S. Schmidt, V. Donzella, A. Sherwali, D. M. Ratner, L. Chrostowski, and K. C. Cheung, "Sub-wavelength grating for enhanced ring resonator biosensor," *Opt. Express*, vol. 24, no. 14, pp. 15672-15686, 2016.
[16] K. Miyamoto, K. Ishibashi, K. Hiroi, Y. Kimura, H. Ishii, and M. Niwano, “Label-free detection and classification of DNA by surface vibration spectroscopy in conjugation with electrophoresis,” *Appl. Phys. Lett.*, vol. 86, pp. 053902, 2005.
[17] F. K. Tittel, Y. Bakhirkin, A. Kosterev, R. Lewicki, S. So, G. Wysocki, and R. F. Curl, “Recent advances and applications of mid-infrared based trace gas sensor technology,” *Proc. SPIE*, vol. 6900, pp. 69000Z, 2008.
[18] M. Sieger and B. Mizaikoff, “Toward On-Chip Mid-Infrared Sensors,” *Anal. Chem.,* vol. 88, no. 11, pp. 5562-5573, 2016.
[19] R. Soref, “Mid-infrared photonics in silicon and germanium,” *Nat. Photonics*, no. 4, pp. 495-497, 2010.
[20] Z. Cheng, X. Chen, C. Y. Wong, K. Xu, C. K. Y. Fung, Y. M. Chen, and H. K. Tsang, "Focusing subwavelength grating coupler for mid-infrared suspended membrane waveguide," *Opt. Lett.*, vol. 37, no. 7, pp. 1217-1219, 2012.
[21] J. S. Penadés, C. A.-Ramos, A. Z. Khokhar, M. Nedeljkovic, L. A. Boodhoo, A. O.-Moñux, I. M.-Fernández, P. Cheben, and G. Z. Mashanovich, "Suspended SOI waveguide with sub-wavelength grating cladding for mid-infrared," *Opt. Lett.*, vol. 39, no. 19, pp. 5661-5664, 2014.
[22] J. S. Penades, A. O.-Moñux, M. Nedeljkovic, J. G. W.-Pérez, R. Halir, A. Z. Khokhar, C. A.-Ramos, Z. Qu, I. M.-Fernández, P. Cheben, and G. Z. Mashanovich, "Suspended silicon mid-infrared waveguide devices with subwavelength grating metamaterial cladding," *Opt. Express*, vol. 24, no. 20, pp. 22908-22916, 2016.
[23] Z. Cheng, X. Chen, C. Y. Wong, K. Xu, and H. K. Tsang, “Mid-infrared Suspended Membrane Waveguide and Ring Resonator on Silicon-on-Insulator,” *IEEE Photon. J.*, vol. 4, no.5, pp. 1510-1519, 2012.
[24] Y. Xia, C. Qiu, X. Zhang, W. Gao, J. Shu, and Q. Xu, "Suspended Si ring resonator for mid-IR application," *Opt. Lett.*, vol. 38, no. 7, pp. 1122-1124, 2013.
[25] H. Sohlström; K. B. Gylfason; D. Hill, “Real-time label-free biosensing with integrated planar waveguide ring resonators,” *Proc. SPIE*, vol. 7719, Silicon Photonics and Photonic Integrated Circuits II, pp. 77190B, 2010.
[26] L. Li and J. J. Burke, “Linear propagation characteristics of periodically segmented waveguides,” *Opt. Lett.*, vol. 17, no. 17, pp. 1195–1197, 1992.
[27] J. D. Bierlein, “Propagation in segmented waveguide structures,” *Quantum Electronics and Laser Science Conference*, p. QTuE2, 1992.
[28] V. Rastogi, V. Mahalakshmi, M. R. Shenoy, K. Thyagarajan, “Propagation characteristics of a novel complementary-structure planar segmented waveguide,” *Optics Communications*, vol. 148, pp. 230-235, 1998.
[29] Z. Weissman and A. Hardy, “Modes of Periodically Segmented Waveguides,” *Journal of Lightwave Technology*, vol. 11, no. 11, 1993.
[30] Z. Weissman and I. Hendel, “Analysis of Periodically Segmented Waveguide Mode Expanders,” *Journal of Lightwave Technology*, vol. 13, no. 10, 1995.
[31] D. Ortega, J. M. Aldariz, J. M. Arnold, and J. S. Aitchison, “Analysis of “Quasi-Modes” in Periodic Segmented Waveguides,” *Journal of Lightwave Technology*, vol. 17, no. 2, 1997.
[32] Z. Weissman, “Evanescent field sensors with periodically segmented waveguides,” *Applied Optics*, vol. 36, no. 6, pp. 1218-1222, 1997.
[33] P. J. Bock, P. Cheben, J. H. Schmid, J. Lapointe, A. Delâge, S. Janz, G. C. Aers, D.-X. Xu, A. Densmore, and T. J. Hall, “Subwavelength grating periodic structures in silicon-on-insulator: a new type of microphotonic waveguide,” *Optics Express*, vol. 18, no. 19, pp. 20251-20262, 2010.
[34] S. Fan, J. D. Joannopoulos, J. N. Winn, A. Devenyi, J. C. Chen, and R. D. Meade, “Guided and defect modes in periodic dielectric waveguides,” *J. Opt. Soc. Am. B*, vol. 12, no. 7, pp. 1267–1272, 1995.
[35] S. F. Helfert and R. Pregla, “Efficient Analysis of Periodic Structures,” *J. Lightwave Technol.*, vol. 16, no. 9, pp. 1694–

1702, 1998.

[36] S. G. Johnson and J. D. Joannopoulos, “Block-iterative frequency-domain methods for Maxwell’s equations in a planewave basis,” *Opt. Express*, vol. 8, no. 3, pp. 173–190, 2001.

[37] J. Ctyroky, S. Helfert, R. Pregla, P. Bienstman, R. Baets, R. De Ridder, R. Stoffer, G. Klaasse, J. Petrac ´ ˇek, P. Lalanne, J. Hugonin, and R. De LaRue, “Bragg waveguide grating as a 1D photonic band gap structure: COST 268 modelling task,” *Opt. Quantum Electron.*, vol. 34, pp. 455–470, 2002.

[38] J. Hugonin, P. Lalanne, I. D. Villar, and I. Matias, “Fourier modal methods for modeling optical dielectric waveguides,” *Opt. Quantum Electron.*, vol. 37, no. 1-3, pp. 107–119, 2005.

[39] G. Lecamp, J. P. Hugonin, and P. Lalanne, “Theoretical and computational concepts for periodic optical waveguides,” *Opt. Express*, vol. 15, no.18, pp. 11042–11060, 2007.

[40] L. Zavargo-Peche, A. Ortega-Monux, J. G. Wanguemert-Perez, and I. Molina-Fernandez, “Fourier based combined techniques to design novel sub-wavelength optical integrated devices,” *Prog. Electromagn. Res.*, vol. 123, pp. 447–465, 2012.

[41] J. Ctyroky, “3-D Bidirectional Propagation Algorithm Based on Fourier Series,” *J. Lightwave Technol.*, vol. 30, no. 23, pp. 3699–3708, 2012.